Ce 4f electronic states of $CeO_{1-x}F_xBiS_2$ studied by soft x-ray photoemission spectroscopy

Takanori Wakita,[1,2,*,†] Kensei Terashima,[1,2,‡] Takahiro Hamada,[1] Hirokazu Fujiwara,[1] Makoto Minohara,[3] Masaki Kobayashi,[3] Koji Horiba,[3] Hiroshi Kumigashira,[3] Galif Kutluk,[4] Masanori Nagao,[5] Satoshi Watauchi,[5] Isao Tanaka,[5] Satoshi Demura,[6,§] Hiroyuki Okazaki,[6,‖] Yoshihiko Takano,[6] Yoshikazu Mizuguchi,[7] Osuke Miura,[7] Kozo Okada,[8] Yuji Muraoka,[1,2,†] and Takayoshi Yokoya[1,2,†]

[1]*Research Laboratory for Surface Science and the Graduate School of Natural Science and Technology, Okayama University, Okayama 700-8530, Japan*

[2]*Research Center of New Functional Materials for Energy Production, Storage, and Transport, Okayama University, Okayama 700-8530, Japan*

[3]*Photon Factory, Institute of Materials Structure Science, High Energy Accelerator Research Organization (KEK), Tsukuba, Ibaraki 305-0801, Japan*

[4]*Synchrotron Radiation Center, Hiroshima University, Kagamiyama, Higashi-Hiroshima 739-0046, Japan*

[5]*Center for Crystal Science and Technology, University of Yamanashi, Kofu, Yamanashi 400-8511, Japan*

[6]*National Institute for Materials Science, Sengen, Tsukuba 305-0047, Japan*

[7]*Department of Electrical and Electronic Engineering, Tokyo Metropolitan University, Minami-osawa, Hachioji 192-0397, Japan*

[8]*Department of Physics and the Graduate school of Natural Science and Technology, Okayama University, Okayama 700-8530, Japan*

(Received 19 November 2015; revised manuscript received 16 December 2016; published 7 February 2017)

We use soft x-ray photoemission spectroscopy (SXPES) to investigate Ce 4f electronic states of a new BiS_2 layered superconductor $CeO_{1-x}F_xBiS_2$, for polycrystalline and single-crystal samples. The Ce 3d spectrum of the single crystal of nominal composition $x = 0.7$ has no f^0 component and the spectral shape closely resembles the ones observed for Ce trivalent insulating compounds, strongly implying that the CeO layer is still in an insulating state even after the F doping. The Ce 3d-4f resonant SXPES for both polycrystalline and single-crystal samples shows that the prominent peak is located around 1 eV below the Fermi level (E_F) with negligible spectral intensity at E_F. The F-concentration dependence of the valence band spectra for single crystals shows the increases of the degeneracy in energy levels and of the interaction between Ce 4f and S 3p states. These results give insight into the nature of the $CeO_{1-x}F_x$ layer and the microscopic coexistence of magnetism and superconductivity in $CeO_{1-x}F_xBiS_2$.

DOI: 10.1103/PhysRevB.95.085109

I. INTRODUCTION

The iron-based superconductors including LnFeAs$O_{1-x}F_x$ (Ln = lanthanide) are discovered in the course of exploring a new p-type transparent semiconductor with two-dimensional layered structure which consists of a narrow-gap semiconductor sandwiched by wide-gap insulating layers [1,2]. LnCuChO (Ch = chalcogen) is one of such transparent semiconductors, and it is pointed out that it has "natural multiple quantum wells" built into its layered structure [3]. For the compounds containing CeO layers as the "wide-gap" layers, such as CeCuSO (Ln = Ce and Ch = S), one of the key issues is the influence of the implantation of the 4f electron into the energy region near the Fermi level (E_F) on the electronic and the magnetic properties. The magnetometry measurement shows that stoichiometric CeCuSO is not a mixed-valence compound but is a well-behaved Ce^{3+} compound [4].

When a narrow-gap semiconductor (CuS) layer in CeCuSO is replaced with a metallic layer consisting of transition metal (TM) and pnictogen (Pn) atoms (Ce$TMPn$O), the interaction between the metallic d band and Ce 4f state leads to diverse variations in the physical properties depending on the strength of the interaction. A typical example is the CeTMPO (TM = Fe, Ru, Os and Pn = P) family of compounds: CeFePO with a paramagnetic heavy fermion behavior [5], CeRuPO with a ferromagnetic (FM) order at $T_C = 15$ K (which is a Kondo lattice system ($T_K \sim 10$ K)) [6], and CeOsPO with an antiferromagnetic (AFM) order at $T_N = 4.4$ K [6]. Another important example is CeFeAsO, which is a bad metal and exhibits a structural distortion near 155 K, followed by a commensurate AFM ordering on the Fe sublattice below ~140 K and an AFM transition of Ce^{3+} below 4 K [7,8]. In addition, the F-doped compound (CeFeAs$O_{1-x}F_x$) shows superconductivity with high transition temperature (as high as $T_c = 41$ K for $x = 0.16$), involved with the suppression of both the structural distortion and the magnetic order [7,8].

$CeO_{1-x}F_xBiS_2$ is one of the newly discovered superconductors LnO$_{1-x}$F$_x$BiS$_2$ (Ln = La, Ce, Pr, Nd, Yb) [9,10] where the $CeO_{1-x}F_x$ and the BiS_2 layers are stacked alternatively. The latter layer has no metallic d band and it is a narrow-gap semiconductor. F substitution for O introduces electron carriers to the BiS_2 layer. Eventually, $CeO_{1-x}F_xBiS_2$ exhibits not only superconductivity but also ferromagnetic-like behaviors

*wakita@cc.okayama-u.ac.jp

†Present address: Research Institute for Interdisciplinary Science (RIIS), Okayama University, Okayama 700-8530, Japan.

‡Present address: Research Institute for Interdisciplinary Science (RIIS), Okayama University, Okayama 700-8530, Japan.

§Present address: Department of Physics, Graduate School of Science, Tokyo University of Science, Kagurazaka, Shinjuku-ku, Tokyo 162-8601, Japan.

‖Present address: Research and Utilization Division, Japan Synchrotron Radiation Research Institute, Kouto, Hyogo 679-5148, Japan.

[11]. Furthermore, it is concluded that the superconducting and the magnetically ordered states coexist for higher x at low temperatures [12–15]. These findings have caused particular interest in this compound and stimulated further investigations of it [16–23]. The phase diagrams, obtained by systematic investigation for nominal F-concentration (x) dependence ($x = 0.0$–1.0) of both the magnetic ordering and the superconducting properties of the as-grown polycrystalline samples, show that ferromagnetic-like ordering occurs at slightly higher temperature than the superconducting transition for $x > 0.4$ [21]. For the samples postannealed under high pressure, the superconducting transition temperature T_c increases and exceeds magnetic ordering temperature T_m to a subtle extent ($T_c \gtrsim T_m$). In contrast, for single-crystal samples, the same trend with the as-grown samples ($T_c < T_m$) is observed. For example, the magnetic ordering temperature T_m is 5.6 K and the superconducting transition temperature T_c (estimated by Meissner effect) is 3.0 K for $x = 0.7$ [19,24]. The Ce L_3 edge x-ray absorption spectroscopy (XAS) measurements for polycrystalline samples show a crossover from mixed valence states to the localized $4f$ states under F doping [16]. The extended x-ray absorption fine structure (EXAFS) analysis exhibits that this change in the electronic structure is driven by suppression of the Ce-S-Bi coupling channel due to the local crystal structure deformation, leading to the coexistence of the superconducting BiS_2 layer and the ferromagnetic $CeO_{1-x}F_x$ layer [16,17]. In contrast, for the $CeOBiS_2$ ($x = 0.0$) single crystal, it is concluded that Ce $4f$ electrons are in a well-localized state split by crystalline-electric-field (CEF) effects, from electrical resistivity, magnetization, and, specific-heat measurements [20].

To reach a comprehensive understanding of these findings, spectroscopic investigation of Ce $4f$ states for single crystals is crucial. Soft x-ray photoemission spectroscopy (SXPES) is known to be a useful experimental technique in order to clarify the nature of Ce $4f$ states [25]. The variety of the physical properties that Ce compounds exhibit (magnetic ordering, heavy fermion, Kondo insulator, mixed valence, and so on) can be explained in terms of the hybridization strength between Ce $4f$ and conduction electrons, which is formulated by single-impurity or periodic-impurity Anderson models. When the hybridization is negligible, Ce $4f$ electrons are localized on the atomic sites and the electronic states of the system can be described with one $4f$ electron (f^1) state and conduction band. The system tends to exhibit magnetic ordering at lower temperature due to RKKY interaction between magnetic moments of $4f$ electrons on the different sites via conduction electrons. As the hybridization increases, $4f$ electrons gain itinerancy and the electronic states can be described with the combination of f^1 and f^0 (no $4f$ electron) states and conduction band. The system can exhibit the Kondo effect and becomes heavy fermions at lower temperature (or insulating behavior, known as a Kondo insulator, because of the formation of the hybridization gap around E_F). When the hybridization is further increased, the system does not show any anomaly and the electronic states can be described by a highly hybridized conduction band, which is explained well with band structure calculations. Such a different electron configuration is reflected in the Ce $3d$ core level photoemission and XAS spectra. More importantly, Ce $3d$-$4f$ resonant SXPES can provide Ce $4f$ partial density of states and therefore directly reveal the relation of Ce $4f$ states with conducting properties, although there are few reports on the Ce $3d$-$4f$ resonant SXPES of layered compounds consisting of alternatively stacked CeO and metallic/semiconducting layers so far [26–28]. Recent reports on Ce $4d$-$4f$ resonant SXPES for $CeO_{1-x}F_xBiS_2$ shows that the Ce $4f$ electrons in both $x = 0.0$ and 0.5 systems respectively formed a flat band at 1.0 and 1.4 eV below E_F and there was no contribution to the Fermi surfaces [29]. Ce $4d$-$4f$ resonant SXPES is, however, surface sensitive and sometimes shows different results from more bulk-sensitive Ce $3d$-$4f$ resonant SXPES [30].

In this study, we report Ce $3d$ core level SXPES, Ce $3d$-$4f$ resonant SXPES, and valence band SXPES results of $CeO_{1-x}F_xBiS_2$ and single crystal ($x = 0.3$ and 0.7) and polycrystalline ($x = 0.7$) samples. The Ce $3d$ spectrum of the single crystal of $x = 0.7$ has no f^0 component and the spectral shape closely resembles the ones observed for Ce trivalent insulating compounds, strongly implying that the CeO layer is still in an insulating state even after the F doping. Ce $3d$-$4f$ resonant SXPES shows that the prominent peak is located around 1 eV below E_F with negligible spectral intensity at E_F, different from the typical spectra characteristic of those in the Kondo regime. This indicates that the Ce $4f$ electrons in the F-doped superconductors play a minor role in the superconductivity. The F-concentration dependence of the valence band spectra of single crystals ($x = 0.3$ and 0.7) shows the enhancements of the degeneracy in the binding energies and of the interaction between Ce $4f$ and S $3p$ states, which strongly support the interpretation that the Ce-S2-Ce superexchange interaction (S2 is an out-of-plane sulfur atom) between Ce^{3+} sites is responsible for the emergence of the magnetic ordering in the $CeO_{1-x}F_x$ layer [16,17,22].

The organization of the paper is as follows. In Sec. II, we describe the sample preparation and the experimental setups. In Sec. III A, we present the Ce $3d$ core level SXPES, and discuss the nature of Ce $4f$ electrons for F-doped compounds. In Sec. III B, we present the resonant SXPES results with Ce $M_{4,5}$ edge XAS spectra and discuss the Ce $4f$ partial density of states. We compare on-resonant SXPES spectra with those of the other systems in Sec. III C. In Sec. III D, we discuss the F-concentration dependence of the valence band spectra and discuss it in terms of local structure deformation. Finally, Sec. IV will contain a summary and conclusions.

II. EXPERIMENTAL

Single-crystal samples of $CeO_{1-x}F_xBiS_2$ were grown by a CsCl/KCl flux method at 873–1073 K in a vacuumed quartz tube [18]. The starting materials were Ce_2S_3, Bi, Bi_2S_3, Bi_2O_3, and BiF_3. The nominal compositions of F were set to be $x = 0.3$ and 0.7, and the chemical compositions (y) were determined to be 0.16 and 0.28 by electron probe microanalysis (EPMA), respectively [24]. For the single crystal of $x = 0.7$, the superconducting transition temperature (T_c) was estimated to be 3.2 K (3.0 K) from the zero-resistivity temperature (from the Meissner effect), while the magnetic ordering temperature (T_m) of 5.6 K was determined as the temperature at which the zero-field-cooled curve begins to deviate from the field-cooled curve. For the single crystal of $x = 0.3$, neither T_c nor T_m were observed above 2 K. Polycrystalline samples of $CeO_{1-x}F_xBiS_2$

were prepared with a solid-state reaction and then annealed under high pressure [21]. Starting materials were Bi_2O_3, BiF_3, Ce_2S_3, Bi_2S_3, and Bi grains. The nominal composition of F was set to be $x = 0.7$. Details on the sample preparation and characterization are given elsewhere [18,19,21,24].

SXPES and XAS measurements were performed at BL-2A in the Photon Factory (PF), KEK, with an SES2002 electron analyzer. The total energy resolution was set to be 0.2–0.4 eV (0.02 eV) for PES measurements using photon energies of 870–1200 eV (70 eV). The binding energies were referenced to E_F of gold. The base pressures of the measurement chambers were better than 2.0×10^{-8} Pa. The samples were fractured (cleaved) for polycrystalline (single-crystal) samples to obtain fresh surfaces at 16 K and kept at the same temperature during the measurements. All SXPES and XAS results reported here were obtained within 8 h after fracturing (cleaving), within which no spectral changes were observed.

III. RESULTS and DISCUSSION

A. Ce 3d SXPES measurement

We start with Ce 3d SXPES in order to obtain insight into the nature of Ce 4f electrons in $CeO_{1-x}F_x$ layers of $CeO_{1-x}F_xBiS_2$. Figure 1 shows Ce 3d SXPES spectra of single-crystal samples, $x = 0.3$ (light green) and 0.7 (dark green), measured with a photon energy of 1200 eV. The $x = 0.3$ spectrum is composed of several peaks that are attributed to the transitions to the three different 4f final states (f^0, f^1, and f^2) for each spin-orbit partner ($3d_{3/2}$ and $3d_{5/2}$). In general, the energy of the f^0 final state in the Ce 3d photoemission process is well separated from those of the other two final states, and so it is considered that the intensity of the highest-binding-energy peak in each set of three structures is a measure of the f^0 component in the initial state [31]. In contrast, the f^1 and f^2 final states have relatively close energies, which results in relatively strong hybridization between them [32]. With increasing x, the intensity of the f^0 peak is reduced and the energy positions of the f^1 and the f^2 peaks show rigid shifts to higher binding energy by 0.3 eV, and the corresponding f^0 component for $3d_{3/2}$ disappears except for a broad structure which may be assigned to a plasmon loss [33]. Here, we cannot completely deny the possibility that the weak f^0 components of $x = 0.3$ originate from the CeO_2-like impurities as discussed in the Supplemental Material [34]. However, we can safely describe an important overall spectral feature, which is not affected by the possible inclusion of CeO_2-like signals which induce the f^0 component; that is, the two-peak structures of f^1 and f^2 components closely resemble the spectra observed for Ce trivalent insulating compounds, such as Ce_2O_3 [35] and $CeCl_3$ [33], but they do not resemble well those for the Ce trivalent metallic compounds such as CeSe [36] and CePd [31] where the f^2 components are weak. These findings strongly imply that the CeO layer is still in an insulating state even after the F doping. For the shoulder structure at ~907 eV, the same structure is observed for $CeCl_3$ [33] and the origin is unclear at present.

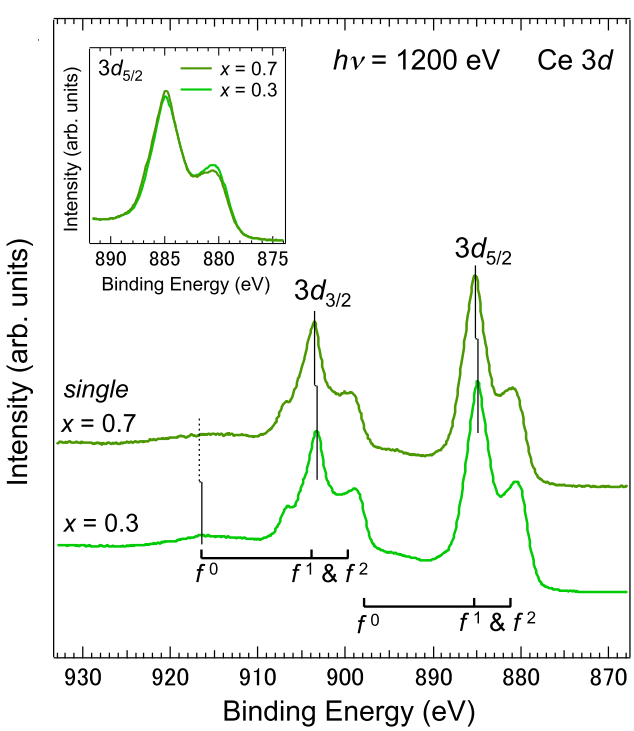

FIG. 1. Ce 3d SXPES spectra of $CeO_{1-x}F_xBiS_2$ single-crystal samples, $x = 0.3$ (light green) and 0.7 (dark green), measured with photon energy of 1200 eV. The inset shows the magnified spectra of the f^1 and f^2 components for $3d_{5/2}$ where the spectra are normalized to the integrated intensities and the spectrum for $x = 0.7$ is shifted by −0.3 eV to match the peak positions with the ones for $x = 0.3$.

The inset shows the magnified spectra of the f^1 and f^2 components for $3d_{5/2}$ where the spectra are normalized to the integrated intensities and the spectrum for $x = 0.7$ is shifted by −0.3 eV to match the peak positions with the ones for $x = 0.3$. It is clear that the width of the spectra are almost the same but the intensity ratio of the two components changes. We will discuss this difference later in Sec. III D, from the view point of the F-concentration dependence of the electronic states.

B. Ce 3d-4f resonant SXPES measurement

A more direct and powerful way to access and reveal the occupied Ce 4f states is to use the Ce 3d-4f resonant SXPES measurement [30,37,38]. This method is selective in chemical states of the target element, and a resonant enhanced spectrum is therefore less influenced by contaminations, especially near the E_F region. In Fig. 2, we show off- and on-resonance spectra of the $x = 0.7$ single-crystal and polycrystalline samples measured at two photon energies, 870 eV (A) and 881.7 eV (B) in XAS spectra near the Ce M_5 edge shown in the inset. Each spectrum is magnified by the scale factor denoted on the right side of the figure.

1. Off-resonant spectra

The off-resonant spectrum (thin curves) for the single-crystal sample of $x = 0.7$ in Fig. 2(a) has dominant structures from 1.5 to 6.5 eV with smaller intensities near the E_F region. The 4f contribution around 1.4 eV (see below) almost vanishes. It should be noted here that this strong reduction

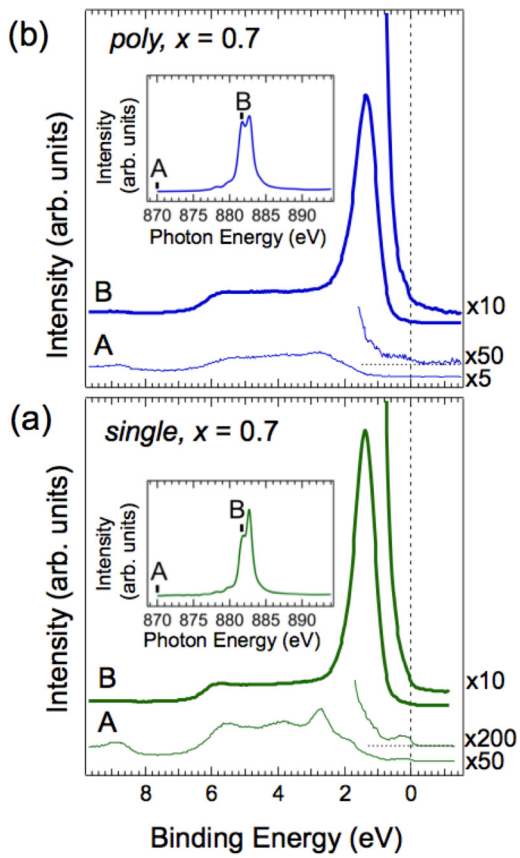

FIG. 2. Ce $3d$-$4f$ resonance SXPES spectra of polycrystalline $CeO_{1-x}F_xBiS_2$ [(a) $x = 0.0$ and (b) 0.7] and the single crystal [(c) $x = 0.7$]. Off- and on-resonance spectra (thin and thick curves, respectively) are measured at two photon energies 870 eV (A) and 881.7 eV (B) in x-ray absorption spectra near the Ce M_5 edge shown in the inset, respectively. Each spectrum is magnified by the scale factor denoted on the right side of the figure.

is due to the Fano profiles and, therefore, can be interpreted as "antiresonance phenomena" [39,40]. The major intensity distributions indicate the partial density of states (pDOS) of O $2p$ and S $3p$ multiplied photoemission cross sections. Actually, the spectral shapes closely resemble the valence band spectra reported for the polycrystalline $LaO_{1-x}F_xBiS_2$ which has no f electron [41]. The band calculation for $LaO_{1-x}F_xBiS_2$ shows that the DOS of the occupied valence states in the lower binding energy region mainly consists of S $3p$ and that in the higher binding energy region mainly originate from O $2p$ [42]. In the magnified off-resonant spectra of near the E_F region in Fig. 2(a), one observes that it has a clear Fermi edge, which is considered that mainly derived from Bi $6p$ states [41,43]. In Fig. 2(b), the off-resonant spectrum for the polycrystalline sample of $x = 0.7$ also shows a similar but more structureless spectral shape with a Fermi edge. These results are consistent with the recent ARPES measurement for a single crystal of $x = 0.7$ which shows a clear Fermi surface [23], although a known unresolved problem that the electrical resistivity measurements exhibit semiconducting behavior still remains [19,24].

2. *On-resonant spectra*

For the on-resonance spectrum (thick curves) in Fig. 2(a), the intensity around 1.4 eV shows a drastic increase while the intensity just near the E_F region stays lower. The on-resonant spectrum for the F-doped polycrystalline sample of $x = 0.7$ in Fig. 2(b) exhibits the same spectral shape as the one in (a), indicating that the on-resonance spectrum for the single crystal in (a) can be regarded as the f pDOS, though normally it reflects the f-derived electronic structure which is integrated only for a limited region in the Brillouin zone (BZ). The absence of the strong enhancement just below the E_F region for both samples indicates that the hybridization of Ce $4f$ electrons and the non-f valence states near the E_F is negligible [44]. This result suggests that Ce $4f$ electrons hardly contribute to the states near the E_F and therefore give a negligible contribution to the superconductivity. This result is, furthermore, consistent with the recent resonant photoemission result for single-crystal $CeO_{0.5}F_{0.5}BiS_2$ using $4d$-$4f$ resonant photoemission [29].

C. Comparison of on-resonant spectra with those for other systems

Comparison of the Ce $4f$ electronic states of $CeO_{1-x}F_xBiS_2$ with other compounds can give further information on the origin of the physical properties. Figure 3 shows the comparison of the on-resonance spectra in Fig. 2 with the ones (black solid curves) of polycrystalline $CeFeAsO_{0.89}F_{0.11}$, single-crystal $CeRhIn_5$, and single-crystal $CeFe_4P_{12}$, which are taken from Refs. [27], [45], and [46], respectively. The energy resolutions used for these spectra have the same order of magnitude (0.2 ∼ 0.3 eV) as the one in this study. The spectra are normalized to the integrated intensities, and the intensity of the $CeFeAsO_{0.89}F_{0.11}$ spectrum is enlarged twice for the sake of clear comparison.

For the single crystal and polycrystalline samples of $CeO_{0.3}F_{0.7}BiS_2$, the peak positions of the main peaks are 1.38 and 1.34 eV, respectively, and the full widths at half maximum (FWHM) of the main peaks (ΔE_{4f}, indicated by arrows) are 0.73 eV and 0.81 eV, respectively. The observed spectral shapes for these two $CeO_{0.3}F_{0.7}BiS_2$ samples have a flat portion with a low intensity from about 2 to 6 eV added to the main peak at 1.3–1.4 eV. The spectral edges around 6 eV have almost the same energy positions with those of the off-resonant spectra (see Fig. 2).

1. *Comparison with* $CeFe_4P_{12}$ *and* $CeRhIn_5$

The observed on-resonant spectra for $CeO_{0.3}F_{0.7}BiS_2$ resemble the one for semiconducting skutterudite $CeFe_4P_{12}$ [46], although the binding energy of the main peak for $CeFe_4P_{12}$ is smaller (at 0.7 eV) and the width of the flat portion in the higher biding energy region is narrower (from 1.5 to 3 eV). The width of the main peak ($\Delta E_{4f} = 0.88$ eV) is slightly broader than the ones for $CeO_{0.3}F_{0.7}BiS_2$. The reason for the small $4f$ derived structure (f^1) near E_F of $CeFe_4P_{12}$ was attributed to the existence of hybridization gap at E_F [46]. This is not the case for the metallic $CeO_{1-x}F_xBiS_2$.

For $CeRhIn_5$, which consists of a metallic Ce layer ($CeIn_3$) and a $RhIn_2$ layer [45], the on-resonant spectrum shows a two-peak spectral structure at E_F and 2 eV in binding

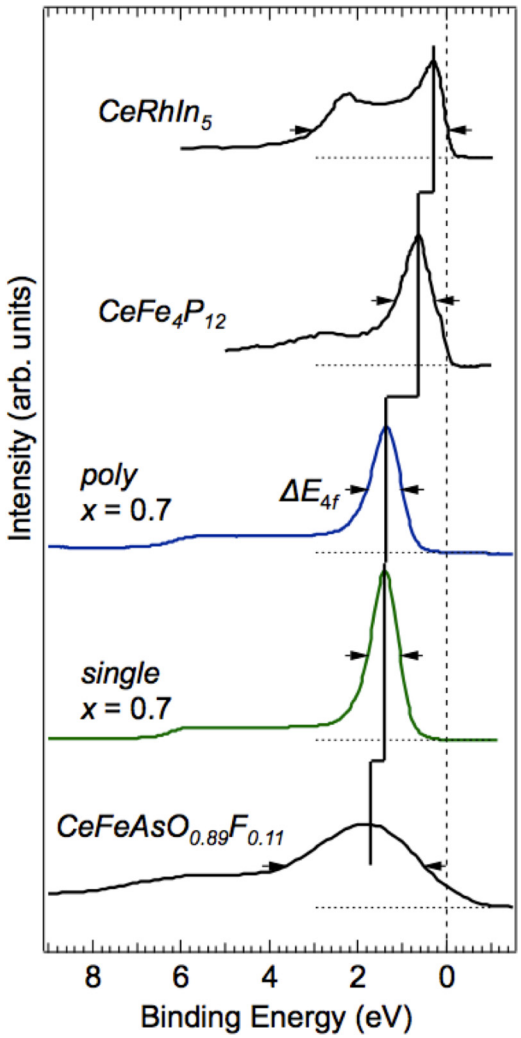

FIG. 3. Comparison of the on-resonance spectra in Fig. 2 with the ones (black solid curves) of polycrystalline $CeFeAsO_{0.89}F_{0.11}$, single-crystal $CeRhIn_5$, and single-crystal $CeFe_4P_{12}$, which are taken from Refs. [27], [45], and [46], respectively. They are normalized to the integrated intensities, and the $CeFeAsO_{0.89}F_{0.11}$ spectrum is enlarged twice for the sake of clarity.

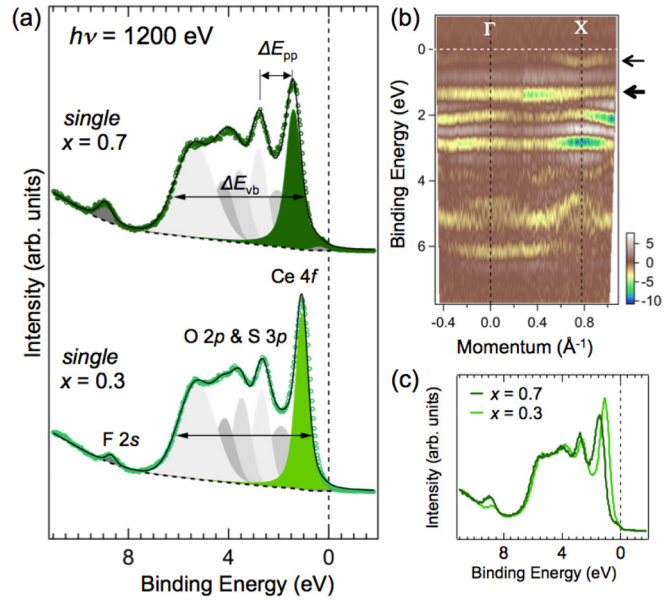

FIG. 4. (a) F-concentration dependence of the valence band spectra of single crystals measured with photon energy of 1200 eV and angle-integrated for acceptance angle of 11 degrees along Γ-X centered at the Γ point (about 200% of the BZ). The nominal concentrations of F (x) are 0.3 and 0.7, respectively. Gray and green Gaussians show fitting results. The dashed lines are assumed Shirley-type backgrounds. (b) Second-derivative intensity map of the energy distribution curves of the ARPES spectra measured along the Γ-X direction for $x = 0.7$ with photon energy of 70 eV. The negatively intense signals show the peak positions of the ARPES spectra. The thick arrow indicates the 4f-derived band and the thin arrow shows the electron pocket band derived mainly from Bi 6p [41,43]. (c) Overlaid comparison of spectra in (a). The spectra are normalized to the integrated intensities.

energy, and the total width of the two-peak spectral shape is about 3.1 eV. This feature is clearly different from that of the on-resonant spectra for $CeO_{0.3}F_{0.7}BiS_2$. $CeRhIn_5$ is regarded as a metallic system with nearly localized 4f and exhibits magnetic ordering at 3.8 K at ambient pressure. The above observation exhibits that the electronic structure of $CeO_{1-x}F_xBiS_2$ is different from that of a metallic Ce layer system with a localized 4f state, though the two compounds have a similar γ values: 58.1 mJ/mol K^2 for the $CeO_{0.5}F_{0.5}BiS_2$ polycrystalline sample [11] and 52 mJ/mol K^2 for $CeRhIn_5$ [47]. This spectral difference also suggests that the magnetic ordering of $CeO_{1-x}F_xBiS_2$ may not be due to RKKY interaction.

2. *Comparison with* $CeFeAsO_{0.89}F_{0.11}$

Regarding $CeFeAsO_{0.89}F_{0.11}$, it has a more similar crystal structure to that of $CeO_{1-x}F_xBiS_2$, consisting of $CeO_{1-x}F_x$ layers between FeAs layers. In Fig. 4, the spectrum of $CeFeAsO_{0.89}F_{0.11}$ has a broad peak around 1.8 eV in binding energy with smaller intensity near E_F, suggesting the negligible hybridization between Ce 4f and the states near E_F. Compared to those of $CeO_{1-x}F_xBiS_2$, that of $CeFeAsO_{0.89}F_{0.11}$ has similar features (a main peak and a flat portion) except that the main peak has a higher binding energy (~1.7 eV) and the whole spectrum is much broader than those of the $CeO_{1-x}F_xBiS_2$ samples. The width of the main peak ΔE_{4f} is 3.1 eV for $CeFeAsO_{0.89}F_{0.11}$, and it is about 4 times larger than those of $CeO_{1-x}F_xBiS_2$ samples. These differences in the on-resonant spectra between the two compounds imply that the hybridization strengths between Ce 4f and other valence states are different in the two compounds, and they seem not to be attributed to differences in the local structures, especially a difference in the Ce-O distances between the two compounds and/or a difference between the Ce-S2 and the Ce-As distances as follows (S2 are out-of-plane sulfur atoms in the BiS_2 layer).

The Ce L_3 edge EXAFS analysis for polycrystalline $CeO_{1-x}F_xBiS_2$ [17] and the neutron scattering analysis for polycrystalline $CeFeAsO_{1-x}F_x$ [8] have revealed that, for nondoped samples, the Ce-O distances in both compounds are 2.34 Å and the Ce-S2(Ce-As) distance is 3.08 Å (3.34 Å). The Ce-O distances are almost the same as the one of CeO_2, 2.36 Å

(discrepancy is 0.85%) [48], while the Ce-S2(Ce-As) distance is about 7% (10%) longer than the Ce-S (Ce-As) distance in a rocksalt CeS (CeAs), 2.89 Å (3.04 Å) [49,50]. These facts suggest that the Ce-O interactions are the same order in both polycrystalline $CeOBiS_2$ and CeFeAsO, and the Ce-S and Ce-As interactions are relatively weaker than the Ce-O interactions in the view points of the bond length. Therefore, the bond length difference seems not to be a main factor of the difference in the hybridization strength between Ce $4f$ and other valence states in the two compounds. Furthermore, upon F-doping to $CeOBiS_2$, the Ce-(O, F) and the Ce-S2 distances in the $CeO_{0.3}F_{0.7}BiS_2$ show relatively large increase (+0.15 Å) and decrease (−0.08 Å), respectively, causing a shift and a broadening in the Ce $4f$ spectrum as discussed later. These changes are, however, small compared with the differences in the on-resonant spectra between $CeO_{1-x}F_xBiS_2$ and $CeFeAsO_{0.89}F_{0.11}$. Incidentally, the Ce-(O, F) and the Ce-As distances in $CeFeAsO_{0.89}F_{0.11}$ exhibit just small changes (less than 0.02 Å) under F doping.

It is therefore considered that the other factor, that is, the energy level alignment between the Ce $4f$ and the S $3p$ (As $4p$), has a more important role in the observed differences between the on-resonant spectra of the two compounds. Here one can obtain valuable information from the valence electronic structure of the rocksalt CeS and CeAs, that is, the Ce $4f$ states in a rocksalt CeS are mostly separated from both of S $3p$ and Ce $5d$ bands and reside in the energy gap between them [51] while the Ce $4f$ states in a rocksalt CeAs are degenerate energetically with the As $4p$ band and merge with it to some extent [52]. This difference between rocksalt CeS and CeAs seems to be a common feature observed between Ce monochalcogenides and monopnictides [51,52]. Similarly, the degeneracy in energy levels between Ce $4f$ and S $3p$ bands in $CeO_{1-x}F_xBiS_2$ is weak, as shown in Fig. 3 where the overlaps between the main peak of the on-resonant spectra and the off-resonant spectra are small, while the occupied states of Ce $4f$ in $CeFeAsO_{0.89}F_{0.11}$ are energetically degenerate with a relatively large part of occupied states of As $4p$ bands as shown by the band calculation and the XES measurements in Ref. [38]. It is therefore considered that, as a result of the above difference in the energy level alignment features, the interaction between the $CeO_{1-x}F_x$ and the BiS_2 layers in $CeO_{1-x}F_xBiS_2$ is weaker than that between the $CeO_{1-x}F_x$ and the FeAs layers in $CeFeAsO_{0.89}F_{0.11}$. This conclusion will be one of the key ingredients to understand the differences in the magnetism and the superconductivity between the two compounds as a whole.

D. F-concentration dependence of the valence band spectra

Finally, we discuss the relation between the structural deformation and the changes in the valence band electronic structure including the Ce $4f$ states caused by the F doping. As noted above, the Ce L_3 edge EXAFS analysis for polycrystalline $CeO_{1-x}F_xBiS_2$ shows that the F doping of $x = 0.7$ results in an increase of the Ce-(O,F) distance by 0.15 Å and a decrease of the Ce-S2 distance by 0.08 Å, accompanied with a decrease of the spacing between the adjacent BiS_2 layers and atomic disorder in the BiS_2 layer [17]. The x-ray diffraction analysis for $CeO_{1-x}F_xBiS_2$ single crystals exhibits that crystals with higher F content have a nearly flat Bi-S plane and that the Ce-(O, F) distance increases from 2.38 to 2.41 Å and the Ce-S2 distance decreases from 3.11 to 3.08 Å under the increase of the F concentration from $x = 0.3$ to 0.7 [19,24]. These trends in the local structural deformations for both polycrystalline and single-crystal samples are consistent with each other.

To elucidate the influences of these local structural deformations on the valence electronic structure precisely, we show the F-concentration dependence of the valence band spectra of single crystals in Fig. 4(a), which are measured with photon energy of 1200 eV and angle-integrated for acceptance angle of 11 degrees along the Γ-X line in the BZ centered at the Γ point (about 200% of BZ along Γ-X line). The use of 1200 eV spectra has an advantage that the Ce derived states and O, S derived states show comparable intensities, which makes it easier to analyze the data, as described below. The nominal concentrations of F (x) are 0.3 and 0.7, respectively, which enable us to link the obtained results with the physical properties. The highest peaks in the spectra correspond to the main peaks in the on-resonant spectra, which means that they are mainly derived from the Ce $4f$ states. In addition, the structures in the higher binding energy region are consistent with the antiresonant spectrum in Fig. 2(a) and attributed to O $2p$ and S $3p$ states. The peaks around 9 eV originate from the F $2s$. These assignments are also confirmed in the second derivative intensity map of the energy distribution curves of the ARPES spectra measured along the Γ-X direction for $x = 0.7$ with photon energy of 70 eV, as shown in Fig. 4(b) where the negatively intense signals show the peak positions of the ARPES spectra. The thick arrow indicates the $4f$-derived band, which is not observed in the ARPES data measured for $LaO_{0.54}F_{0.46}BiS_2$ [53]. The thin arrow shows the electron pocket band derived mainly from Bi $6p$ [41,43].

Under the increase of the F concentration from $x = 0.3$ to 0.7, the spectrum does not show a complete rigid shift, as seen in Fig. 4(c) (where the spectra are normalized to the integrated intensities). The most intense peak (Ce $4f$) shifts by 0.3 eV which corresponds to the shift of the Ce $3d$ spectrum (see Fig. 1), while the other structures in the higher binding energy region (including S $3p$, O $2p$, and F $2s$) shift by 0.2 eV. The latter shift is almost rigid, suggesting a close relation with the chemical potential shift due to the carrier doping. As a result of the additional shift of the Ce $4f$ peak (0.3–0.2 = 0.1 eV), the peak-to-peak energy separation between the most and the second most intense peaks (ΔE_{pp}) changes from 1.5 eV to 1.4 eV. Simultaneously, the valence-band width (ΔE_{VB}), which is the energy width of the whole band (including Ce $4f$, S $3p$, and O $2p$) at the half maximum of the higher binding energy edge indicated by arrows, also decreases from 5.6 eV to 5.4 eV. In contrast, the width of the most intense peak (ΔE_{4f}) increases slightly from 0.73 eV to 0.77 eV, which is confirmed by the fitting procedure with Gaussian functions as shown in Fig. 4(a). This small broadening of ΔE_{4f} may related to the increase of the adjacent F atoms which will modify the potential energy on the Ce site, producing the site variation of the $4f$ states. This site variation may affect also the width and shape of the Ce $3d$ spectra, although the changes will be expected to be small because of the small changes in ΔE_{4f}. Actually, the Ce $3d$ spectra in Fig. 1 shows almost the same width with each other. The intensity ratio of

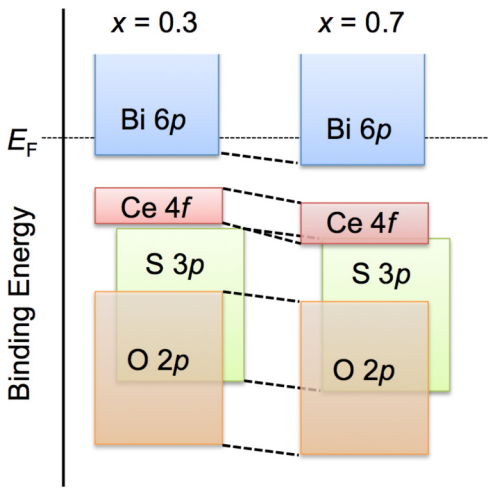

FIG. 5. Schematic picture of F-concentration dependencies of the valence bands.

the f^1 and f^2 components, however, exhibits clear difference as mentioned in Sec. III A. According to the results obtained by the Ce-ligand cluster model calculation [32], this kind of change in the intensity ratio of the f^1 and f^2 components can be interpreted as a result of the changes in the energy separation between Ce 4f and the ligand (O 2p and S 3p) states and of those in the interaction between them. In fact, these changes are observed as the additional shift of the Ce 4f peak (the decrease of ΔE_{pp}) and the reduction of ΔE_{VB}. Here we present an interpretation which can explain the derivation of these changes in the valence bands as a whole, in the view point of the structural deformation resulting from the increase of the F concentration; the increase of the Ce-(O, F) distance upon F doping weakens the interaction between Ce 4f and O 2p states, and it causes a decrease of the energy separation of bonding and antibonding states consisting of them, leading to the decreases of the ΔE_{pp} and the ΔE_{VB}. The decrease of the ΔE_{pp}, then, enhances the interaction between Ce 4f and S 3p states together with the decrease of the Ce-S2 distance under the F doping. This increase of the interaction between Ce 4f and S 3p states possibly results in just a slight increase of the ΔE_{4f} as observed, since the interaction between Ce 4f and S 3p states is relatively weak due to the 7% longer Ce-S distance than that of a rocksalt CeS. These F-concentration dependencies of the valence bands are depicted schematically in Fig. 5. It should be noted here that the observed increases of the degeneracy in energy levels and of the interaction between Ce 4f and S 3p states strongly support the interpretation that the Ce-S2-Ce superexchange interaction between Ce^{3+} sites is responsible for the emergence of the magnetic ordering in the $CeO_{1-x}F_x$ layer, explaining the absence ($x = 0.3$) and presence ($x = 0.7$) of the magnetic ordering [16,17,22]. In addition, the Ce 4f peak shifting from the E_F under F doping suggests that the magnetic ordering and the superconductivity are disconnected in this system. We hope that the present results motivate further theoretical investigation to confirm this scenario for the magnetic ordering and the superconductivity.

IV. CONCLUSIONS

We have performed Ce 3d core level SXPES, Ce $M_{4,5}$ edge XAS, and Ce 3d-4f resonant SXPES to study electronic structure of Ce 4f electrons for $CeO_{1-x}F_xBiS_2$ polycrystalline ($x = 0.0$ and 0.7) and single-crystal samples ($x = 0.3$ and 0.7). The Ce 3d spectrum of the single crystal of $x = 0.7$ has no f^0 component and the spectral shape closely resembles the ones observed for Ce trivalent insulating compounds, strongly implying that the CeO layer is still in an insulating state even after the F doping. From 3d-4f resonant SXPES, negligible Ce 4f contribution to states at E_F is observed, indicating that Ce 4f plays a minor role in metallic/superconducting properties. The very different spectral shape of $CeO_{1-x}F_xBiS_2$ compared to that of a Ce compound having localized Ce 4f and exhibiting magnetism suggests that the origin of the magnetic ordering in $CeO_{1-x}F_xBiS_2$ may not be due to RKKY interaction. The comparison of the on-resonant spectra with the one for $CeFeAsO_{0.89}F_{0.11}$ shows that the interaction between the $CeO_{1-x}F_x$ and the BiS_2 layers in $CeO_{1-x}F_xBiS_2$ is weaker than that between the $CeO_{1-x}F_x$ and the FeAs layers in $CeFeAsO_{0.89}F_{0.11}$. The F-concentration dependence of the valence band spectra of single crystals ($x = 0.3$ and 0.7) shows the increases of the degeneracy in energy levels and of the interaction between Ce 4f and S 3p states under F doping, which strongly support the interpretation that the Ce-S2-Ce superexchange interaction between Ce^{3+} sites is responsible for the emergence of the magnetic ordering in the $CeO_{1-x}F_x$ layer. These results give insight into the nature of the $CeO_{1-x}F_x$ layer and the microscopic coexistence of magnetism and superconductivity in $CeO_{1-x}F_xBiS_2$.

ACKNOWLEDGMENTS

PES measurements at BL-2A of PF were performed under Project No. 2015S2-005. Preliminary measurements were formed at SPring-8 (2013B1649). This work was partially supported by JSPS KAKENHI Grant No. 15H03691. This work was also partially supported by the Program for Promoting the Enhancement of Research Universities from MEXT.

[1] H. Hosono, J. Phys. Soc. Jpn. Suppl. C **77**, 1 (2008).
[2] Y. Kamihara, T. Watanabe, M. Hirano, and H. Hosono, J. Am. Chem. Soc. **130**, 3296 (2008).
[3] K. Ueda, H. Hiramatsu, H. Ohta, M. Hirano, T. Kamiya, and H. Hosono, Phys. Rev. B **69**, 155305 (2004).
[4] M. J. Pitcher, C. F. Smura, and S. J. Clarke, Inorg. Chem. **48**, 9054 (2009).
[5] E. M. Brüning, C. Krellner, M. Baenitz, A. Jesche, F. Steglich, and C. Geibel, Phys. Rev. Lett. **101**, 117206 (2008).
[6] C. Krellner, N. S. Kini, E. M. Brüning, K. Koch, H. Rosner, M. Nicklas, M. Baenitz, and C. Geibel, Phys. Rev. B **76**, 104418 (2007).
[7] G. F. Chen, Z. Li, D. Wu, G. Li, W. Z. Hu, J. Dong, P. Zheng, J. L. Luo, and N. L. Wang, Phys. Rev. Lett. **100**, 247002 (2008).

[8] J. Zhao, Q. Huang, C. De La Cruz, S. Li, J. Lynn, Y. Chen, M. A. Green, G. Chen, G. Li, Z. Li, J. L. Luo, N. L. Wang, and P. Dai, Nat. Mater. **7**, 953 (2008).
[9] Y. Mizuguchi, J. Phys. Chem. Solids **84**, 34 (2015).
[10] D. Yazici, I. Jeon, B. White, and M. Maple, Physica C **514**, 218 (2015).
[11] D. Yazici, K. Huang, B. White, A. Chang, A. Friedman, and M. Maple, Philos. Mag. **93**, 673 (2013).
[12] J. Xing, S. Li, X. Ding, H. Yang, and H.-H. Wen, Phys. Rev. B **86**, 214518 (2012).
[13] R. Jha and V. P. S. Awana, J. Supercond. Novel Magn. **27**, 1 (2014).
[14] C. T. Wolowiec, D. Yazici, B. D. White, K. Huang, and M. B. Maple, Phys. Rev. B **88**, 064503 (2013).
[15] J. Lee, S. Demura, M. B. Stone, K. Iida, G. Ehlers, C. R. dela Cruz, M. Matsuda, K. Deguchi, Y. Takano, Y. Mizuguchi, O. Miura, D. Louca, and S.-H. Lee, Phys. Rev. B **90**, 224410 (2014).
[16] T. Sugimoto, B. Joseph, E. Paris, A. Iadecola, T. Mizokawa, S. Demura, Y. Mizuguchi, Y. Takano, and N. L. Saini, Phys. Rev. B **89**, 201117(R) (2014).
[17] E. Paris, B. Joseph, A. Iadecola, T. Sugimoto, L. Olivi, S. Demura, Y. Mizuguchi, Y. Takano, T. Mizokawa, and N. Saini, J. Phys.: Condens. Matter **26**, 435701 (2014).
[18] M. Nagao, A. Miura, S. Demura, K. Deguchi, S. Watauchi, T. Takei, Y. Takano, N. Kumada, and I. Tanaka, Solid State Commun. **178**, 33 (2014).
[19] A. Miura, M. Nagao, T. Takei, S. Watauchi, Y. Mizuguchi, Y. Takano, I. Tanaka, and N. Kumada, Cryst. Growth Des. **15**, 39 (2014).
[20] R. Higashinaka, T. Asano, T. Nakashima, K. Fushiya, Y. Mizuguchi, O. Miura, T. D. Matsuda, and Y. Aoki, J. Phys. Soc. Jpn. **84**, 023702 (2014).
[21] S. Demura, K. Deguchi, Y. Mizuguchi, K. Sato, R. Honjyo, A. Yamashita, T. Yamaki, H. Hara, T. Watanabe, S. J. Denholme, M. Fujioka, H. Okazaki, T. Ozaki, O. Miura, T. Yamaguchi, H. Takeya, and Y. Takano, J. Phys. Soc. Jpn. **84**, 024709 (2015).
[22] T. Sugimoto, B. Joseph, E. Paris, A. Iadecola, S. Demura, Y. Mizuguchi, Y. Takano, T. Mizokawa, and N. L. Saini, J. Phys.: Conf. Ser. **592**, 012073 (2015).
[23] T. Sugimoto, D. Ootsuki, C. Morice, E. Artacho, S. S. Saxena, E. F. Schwier, M. Zheng, Y. Kojima, H. Iwasawa, K. Shimada, M. Arita, H. Namatame, M. Taniguchi, M. Takahashi, N. L. Saini, T. Asano, R. Higashinaka, T. D. Matsuda, Y. Aoki, and T. Mizokawa, Phys. Rev. B **92**, 041113(R) (2015).
[24] M. Nagao, Nov. Supercond. Mater. **1**, 64 (2015).
[25] A. Sekiyama, S. Imada, A. Yamasaki, and S. Suga, in *Very High Resolution Photoelectron Spectroscopy*, edited by S. Hüfner (Springer-Verlag, Berlin, 2007), pp. 351–372.
[26] H. Sato, S. Nishimoto, K. Takase, H. Nakao, K. Yoshikawa, M. Higashi, M. Taniguchi, H. Negishi, S. Negishi, Y. Takahashi, Y. Takano, and K. Sekizawa, Phys. Status Solidi C **3**, 2884 (2006).
[27] F. Bondino, E. Magnano, M. Malvestuto, F. Parmigiani, M. A. McGuire, A. S. Sefat, B. C. Sales, R. Jin, D. Mandrus, E. W. Plummer, D. J. Singh, and N. Mannella, Phys. Rev. Lett. **101**, 267001 (2008).
[28] M. G. Holder, A. Jesche, P. Lombardo, R. Hayn, D. V. Vyalikh, S. Danzenbächer, K. Kummer, C. Krellner, C. Geibel, Y. Kucherenko, T. K. Kim, R. Follath, S. L. Molodtsov, and C. Laubschat, Phys. Rev. Lett. **104**, 096402 (2010).
[29] T. Sugimoto, D. Ootsuki, E. Paris, A. Iadecola, M. Salome, E. F. Schwier, H. Iwasawa, K. Shimada, T. Asano, R. Higashinaka, T. D. Matsuda, Y. Aoki, N. L. Saini, and T. Mizokawa, Phys. Rev. B **94**, 081106(R) (2016).
[30] A. Sekiyama, T. Iwasaki, K. Matsuda, Y. Saitoh, Y. Onuki, and S. Suga, Nature (London) **403**, 396 (2000).
[31] J. C. Fuggle, F. U. Hillebrecht, Z. Zolnierek, R. Lässer, C. Freiburg, O. Gunnarsson, and K. Schönhammer, Phys. Rev. B **27**, 7330 (1983).
[32] A. Fujimori, Phys. Rev. B **27**, 3992 (1983).
[33] K.-H. Park and S.-J. Oh, Phys. Rev. B **48**, 14833 (1993).
[34] See Supplemental Material at http://link.aps.org/supplemental/10.1103/PhysRevB.95.085109 for Ce 3*d* SXPES and Ce $M_{4,5}$-edge XAS spectra of $CeO_{1-x}F_xBiS_2$ polycrystalline and single crystal samples.
[35] J. W. Allen, J. Magn. Magn. Mater. **47-48**, 168 (1985).
[36] R. Lässer, J. C. Fuggle, M. Beyss, M. Campagna, F. Steglich, and F. Hulliger, Physica B+C **102**, 360 (1980).
[37] A. Sekiyama and S. Suga, Physica B **312-313**, 634 (2002).
[38] F. Bondino, E. Magnano, C. H. Booth, F. Offi, G. Panaccione, M. Malvestuto, G. Paolicelli, L. Simonelli, F. Parmigiani, M. A. McGuire, A. S. Sefat, B. C. Sales, R. Jin, P. Vilmercati, D. Mandrus, D. J. Singh, and N. Mannella, Phys. Rev. B **82**, 014529 (2010).
[39] T. Iwasaki, S. Suga, S. Imada, A. Sekiyama, K. Matsuda, M. Kotsugi, K.-S. An, T. Muro, S. Ueda, T. Matsushita, Y. Saitoh, T. Nakatani, H. Ishii, O. Sakai, R. Takayama, T. Suzuki, T. Oguchi, K. Katoh, and A. Ochiai, Phys. Rev. B **61**, 4621 (2000).
[40] S. Banik, A. Chakrabarti, D. A. Joshi, A. Thamizhavel, D. M. Phase, S. K. Dhar, and S. K. Deb, Phys. Rev. B **82**, 113107 (2010); W. Gudat, R. Rosei, J. Weaver, E. Kaldis, and F. Hulliger, Solid State Commun. **41**, 37 (1982).
[41] S. Nagira, J. Sonoyama, T. Wakita, M. Sunagawa, Y. Izumi, T. Muro, H. Kumigashira, M. Oshima, K. Deguchi, H. Okazaki, Y. Takano, O. Miura, Y. Mizuguchi, K. Suzuki, H. Usui, K. Kuroki, K. Okada, Y. Muraoka, and T. Yokoya, J. Phys. Soc. Jpn. **83**, 033703 (2014).
[42] B. Li, Z. Xing, and G. Huang, Europhys. Lett. **101**, 47002 (2013).
[43] H. Usui, K. Suzuki, and K. Kuroki, Phys. Rev. B **86**, 220501(R) (2012).
[44] In general, there is a possibility that one can observe different resonant behaviors for the different final states. For Ce compounds classified into a Kondo system, however, the Kondo resonance peak of the Ce 4*f* state is observed with the maximum intensity at the photon energy corresponding to one of the main peaks in their Ce M_5 edge XAS spectrum, since both of the intermediate states of the Kondo resonance peak and the final state of the main structure of the Ce M_5 edge XAS spectrum are the same state, that is, $3d^94f^2$. To see the presence or absence of a Kondo resonance, it is important to measure the spectrum at the photon energy of the maximum resonance enhancement. We have observed the maximum intensity for the spectrum measured at the photon energy B among the resonance spectra measured at the several photon energies (not shown).
[45] S.-I. Fujimori, T. Okane, J. Okamoto, K. Mamiya, Y. Muramatsu, A. Fujimori, H. Harima, D. Aoki, S. Ikeda, H. Shishido, Y. Tokiwa, Y. Haga, and Y. Ōnuki, Phys. Rev. B **67**, 144507 (2003).

[46] M. Matsunami, K. Horiba, M. Taguchi, K. Yamamoto, A. Chainani, Y. Takata, Y. Senba, H. Ohashi, M. Yabashi, K. Tamasaku, Y. Nishino, D. Miwa, T. Ishikawa, E. Ikenaga, K. Kobayashi, H. Sugawara, H. Sato, H. Harima, and S. Shin, Phys. Rev. B **77**, 165126 (2008).

[47] G. Knebel, M. Measson, B. Salce, D. Aoki, D. Braithwaite, J. Brison, and J. Flouquet, J. Phys.: Condens. Matter **16**, 8905 (2004).

[48] G. Dutta, U. V. Waghmare, T. Baidya, M. Hegde, K. Priolkar, and P. Sarode, Catal. Lett. **108**, 165 (2006).

[49] A. Dönni, A. Furrer, P. Fischer, and F. Hulliger, Physica B **186-188**, 541 (1993).

[50] A. Aeby, F. Hulliger, and B. Natterer, Solid State Commun. **13**, 1365 (1973).

[51] M. Nakayama, H. Aoki, A. Ochiai, T. Ito, H. Kumigashira, T. Takahashi, and H. Harima, Phys. Rev. B **69**, 155116 (2004).

[52] Y. Baer, R. Hauger, C. Zürcher, M. Campagna, and G. K. Wertheim, Phys. Rev. B **18**, 4433 (1978).

[53] K. Terashima, J. Sonoyama, T. Wakita, M. Sunagawa, K. Ono, H. Kumigashira, T. Muro, M. Nagao, S. Watauchi, I. Tanaka, H. Okazaki, Y. Takano, O. Miura, Y. Mizuguchi, H. Usui, K. Suzuki, K. Kuroki, Y. Muraoka, and T. Yokoya, Phys. Rev. B **90**, 220512(R) (2014).